Causality detection in cortical seizure dynamics using cross-dynamical delay differential analysis

Cite as: Chaos **29**, 101103 (2019); doi: 10.1063/1.5126125
Submitted: 29 August 2019 · Accepted: 17 September 2019 ·
Published Online: 8 October 2019

Claudia Lainscsek,[1,2,a] Christopher E. Gonzalez,[1,3,a] Aaron L. Sampson,[1,3] Sydney S. Cash,[4] and Terrence J. Sejnowski[1,2,5]

AFFILIATIONS

[1]Computational Neurobiology Laboratory, The Salk Institute for Biological Studies, 10010 North Torrey Pines Road, La Jolla, California 92037, USA
[2]Institute for Neural Computation, University of California San Diego, La Jolla, California 92093, USA
[3]Department of Neurosciences, University of California San Diego, La Jolla, California 92093, USA
[4]Department of Neurology, Massachusetts General Hospital and Harvard Medical School, Boston, Massachusetts 02114, USA
[5]Division of Biological Sciences, University of California San Diego, La Jolla, California 92093, USA

[a]**Contributions:** C. Lainscsek and C. E. Gonzalez contributed equally to this work.

ABSTRACT

Most natural systems, including the brain, are highly nonlinear and complex, and determining information flow among the components that make up these dynamic systems is challenging. One such example is identifying abnormal causal interactions among different brain areas that give rise to epileptic activities. Here, we introduce cross-dynamical delay differential analysis, an extension of delay differential analysis, as a tool to establish causal relationships from time series signals. Our method can infer causality from short time series signals as well as in the presence of noise. Furthermore, we can determine the onset of generalized synchronization directly from time series data, without having to consult the underlying equations. We first validate our method on simulated datasets from coupled dynamical systems and apply the method to intracranial electroencephalography data obtained from epilepsy patients to better characterize large-scale information flow during epilepsy.

Establishing and detecting information flow in a complex system with many interacting components is challenging yet crucial for many scientific fields. Currently available methods for inferring directionality and causality from observed time series signals are often limited by the number of data required and computational processing time. In this study, we present an efficient and accurate method for measuring causal interaction. We demonstrate that our method, cross-dynamical delay differential analysis (CD-DDA), can estimate the magnitude and direction of information flow in simulated datasets accurately. Furthermore, we applied our method to brain signals obtained from epilepsy patients to characterize previously unidentified seizure-related information flow.

I. INTRODUCTION

Determination of causality and direction of information flow is fundamental to various fields of science, from neuroscience to climate research. In neuroscience, for example, information flow and the nonlinear dynamical causal architecture in brain electroencephalography (EEG) data are important for understanding and predicting events (e.g., seizures). Various regions in the brain might be causally connected even if the data from those regions do not show strong correlations. This might be due to the spatiotemporal nonstationarity of the system.

As pointed out by Yule in 1926,[36] correlation does not imply causation. Yule also made a connection between the introduction of delays and causal relations between time series. In 1969, Granger[10] introduced a statistical measure of causality that is widely used in signal processing. This work is closely related to the work of Wiener, which was published in 1956.[35] Since Granger causality (GC) relies on linear autoregressive models, it may not yield good results for some nonlinear systems. To circumvent the limitations of the linear Granger causality test, Brock *et al.*[8,9] proposed a test based on correlation integrals[11] and Baek and Brock,[3] Hiemstra and Jones,[12] and Bai *et al.*[4,5] and then introduced nonlinear Granger causality. In 2000, Schreiber[32] introduced transfer entropy for information transfer between nonlinear dynamical systems. If the systems are linear Gaussian processes, GC and transfer entropy are equivalent.[6] Determining causality from dynamical attractors of nonlinear dynamical systems

and the concept of generalized synchronization (GS) were introduced by Schiff *et al.*,[31] Arnhold *et al.*,[2] Hirata *et al.*,[13,14] and Sugihara *et al.*,[33] among others. One implementation is Sugihara's convergent cross-mapping (CCM).[33] CCM is based on standard uniform delay embeddings and is, therefore, limited to a subset of the dynamical systems found in nature. In 2018, a focus issue in Chaos was published that summarizes recent developments for causality detection.[7] Recent articles used complex network theory to characterize causality of multivariate data.[28,37]

Here, we determine causality through nonlinear, nonuniform, functional embeddings as an extension of delay differential analysis (DDA) and call this method *cross-dynamical DDA* (CD-DDA). We first test CD-DDA on simulated data from coupled dynamical systems and then apply this analysis to investigate spatiotemporal information flow in the brain before and during seizures.

This paper is organized as follows: Sec. II introduces classical DDA and the extension to CD-DDA to study causality. In Sec. III, causal interactions of coupled Lorenz and Rössler systems are investigated. In Sec. IV, CD-DDA is applied to epileptic seizures. Section V is the conclusion.

II. DETECTING CAUSALITY USING DELAY DIFFERENTIAL ANALYSIS (DDA)

DDA combines differential embeddings with linear and nonlinear nonuniform functional delay embeddings[22,30,34] to relate the current derivatives of a system to the current and past values of the system variables.[15,18] Inspired by Max Planck's "natural units,"[25] the DDA model maps experimental data onto a set of natural embedding coordinates.

The general nonlinear DDA model is

$$\dot{u} = \sum_{i=1}^{I} a_i \prod_{n=1}^{N} u_{\tau_n}^{m_{n,i}} + \rho_u = \mathcal{F}_u + \rho_u \tag{1}$$

for $\tau_n, m_{n,i} \in \mathbb{N}_0$, where N is the number of delays (usually 2), I is the number of terms (typically around 3), and $u_{\tau_n} = u(t - \tau_n)$, relating the signal derivative $\dot{u}$ to the signal nonuniformly shifted in time. We then use the coefficients a_i and the least square error ρ_u as features. Note that we explicitly added ρ_u to highlight its use in the causal DDA measure introduced below. To restrict complexity of the DDA model, most of the terms in Eq. (1) are set to zero. We, therefore, consider here DDA models with two delays τ_n, three terms, and a degree $\sum_i m_{n,i} \leq 4$ of nonlinearity.

To put DDA in context, a general nonlinear, real-valued function can be expressed in a Taylor series expansion of functionals of increasing complexity around some fixed point. When the function $F(\star)$ represents the behavior of a dynamical system, that is, a time series model where the input is formed from past inputs $[u(t), u(t-\tau_1), \ldots]$, the expansion becomes a Volterra series. We have

$$\begin{aligned}\dot{u} = \mathbf{u}_0 &+ \sum_{i=0}^{\infty} g_i \mathbf{u}_{\tau_i} + \sum_{i_1=0}^{\infty}\sum_{i_2=0}^{\infty} g_{i_1,i_2} \mathbf{u}_{\tau_{i_1}} \mathbf{u}_{\tau_{i_2}} \\ &+ \cdots \\ &+ \sum_{i_1=0}^{\infty}\sum_{i_2=0}^{\infty}\cdots\sum_{i_q=0}^{\infty} g_{i_1,i_2,\ldots,i_q} \mathbf{u}_{\tau_{i_1}} \mathbf{u}_{\tau_{i_2}} \cdots \mathbf{u}_{\tau_q},\end{aligned} \tag{2}$$

with the linear and nonlinear data components modeled as separate model terms. To find a model that is a projection onto a stable manifold, we consider low-order models composed of a finite number of leading terms in Eq. (2), such as Eq. (1). This makes CD-DDA different to GC since we use (1) a derivative on the left side of the equation instead of the time series itself in GC, (2) nonuniform functional embeddings on the right side of the equation that were selected from the data instead of uniform linear embeddings of lags 1,2,…in GC, (3) two delays instead of a chain of around 10–15 delays in GC, and (4) three term models that are selected to fit each time series instead of around 15 general terms.

To be more explicit, let us give an example. A typical DDA model for the analysis of EEG and intracranial EEG (iEEG) data is the three term model [all a_i in Eq. (1) except three are set to zero]:

$$\dot{u} = a_1 u_1 + a_2 u_2 + a_3 u_1^4 + \rho_u\,, \tag{3}$$

where $u(t)$ is the time series from one EEG channel and $u_i = u(t - \tau_i)$. The derivative on the left side is computed using a 5-point center derivative algorithm.[21] The coefficients a_i are estimated with numerical singular value decomposition (SVD) to minimize the least square error.[26] The DDA model that best fits the overall dynamical properties of the system [e.g., (3) for EEG data] can be found by supervised (maximizing the classification performance) or unsupervised (minimizing the least square error ρ) structure selection from a list of candidate models (see, e.g., Refs. 18 and 17).

DDA is a nonlinear data analysis framework that (1) uses unprocessed data so as not to disturb the nonlinear properties of the data, (2) uses sparse models that match the macroscopic architecture of the underlying dynamical system, (3) disregards amplitude information to concentrate on the dynamical aspects of the data, and (4) can be extended for detection of dynamical causality in the data to understand information flow in the system. Previously, it has been demonstrated that DDA captures essential features of data to produce exceptional classification performance.

Let us consider two dynamical systems from which the time series $u(t)$ and $v(t)$ are measured, respectively. In order to consider whether there is a causal interaction between these two time series, we start by looking for a model

$$\dot{u} = \mathcal{F}_u + \rho_u, \tag{4}$$

minimizing the error for the time series u. We also minimize the error for $v(t)$ and get

$$\dot{v} = \mathcal{F}_v + \rho_v. \tag{5}$$

If we assume, for example, a unidirectional causal influence of $u(t)$ on $v(t)$,

$$\dot{u} = \mathcal{F}_u + \mathcal{F}_v + \rho_{uv}, \tag{6}$$

the errors ρ_u and ρ_{uv} should be similar since the coefficients of $\mathcal{F}_v$ are irrelevant. In contrast, for

$$\dot{v} = \mathcal{F}_v + \mathcal{F}_u + \rho_{vu}, \tag{7}$$

the errors ρ_v and ρ_{vu} are different.

We then define $\mathcal{C}_{uv}$ as our CD-DDA measure of the causal influence of $v(t)$ on $u(t)$ and $\mathcal{C}_{vu}$ for a causal influence of $u(t)$ on $v(t)$,

$$\mathcal{C}_{uv} = |\rho_u - \rho_{uv}|; \quad \mathcal{C}_{vu} = |\rho_v - \rho_{vu}|. \tag{8}$$

We additionally use the significance $\frac{\mu}{\sigma}$, where μ is the mean and σ is the standard deviation, of the estimated coefficients of the terms $\mathcal{F}_v$ in Eq. (6) and $\mathcal{F}_u$ in Eq. (7) to estimate the synchronization level, $\mathcal{S}$.

III. APPLICATIONS TO SIMULATED DATA

To test CD-DDA, we generate simulated data from coupled Rössler[27] and Lorenz[20] systems. The first example was previously studied in Ref. 24 and is an autonomous, chaotic Rössler system driving a periodic Rössler system. Our second simulated example is a Rössler system driving a Lorenz system.[19,23,24] For the coupled Rössler system, the functions $\mathcal{F}_u$ and $\mathcal{F}_v$ are the same. For the coupled Rössler and Lorenz system, we need to select individual functions $\mathcal{F}_u$ and $\mathcal{F}_v$ since these two systems are dynamically different.

We compared our measure with linear Granger causality,[10] transfer entropy or conditional mutual information,[32] and convergent cross-mapping[33] for a chaotic Rössler system driving a periodic Rössler system and for a Rössler system driving a Lorenz system. Our measure performed as well or better than the other three measures for both of these systems, and we report these findings in Figs. 2 and 4 in the supplementary material.

A. Chaotic Rössler system driving a periodic Rössler system

In this example, we unidirectionally couple two Rössler systems, where the driving system $\boldsymbol{R_1}$ is chaotic and the driven system $\boldsymbol{R_2}$ is periodic[24]

$$\begin{aligned} \boldsymbol{R_1} &\begin{cases} \dot{x}_1 = -\omega_1 y_1 - z_1, \\ \dot{y}_1 = x_1 + a\, y_1, \\ \dot{z}_1 = b + z_1(x_1 - c), \end{cases} \\ \boldsymbol{R_2} &\begin{cases} \dot{x}_2 = -\omega_2 y_2 - z_2 + \epsilon(x_1 - x_2), \\ \dot{y}_2 = x_2 + a\, y_2, \\ \dot{z}_2 = b + z_2(x_2 - c), \end{cases} \end{aligned} \tag{9}$$

with $a = 0.15$, $\omega_1^2 = 1.015$, $\omega_2^2 = 0.985$, $b = 0.2$, and $c = 10$. We modified the system in Ref. 24 to the system above as explained in the Appendix. The coupling strength ϵ was varied between 0 and 0.25 using 30 000 linearly spaced steps. The integration step size was set to 0.05 with a transient of 10^5 time points discarded. The remaining data were downsampled by a factor of 2 resulting in 10^5 data points for each coupling strength.

We selected the DDA models by minimizing the model error ρ_u from $u = x_1$ or $u = x_2$ and get

$$\mathcal{F}_u = a_1\, u_1 + a_2\, u_2 + a_3\, u_1^3, \tag{10}$$

with $u_j = u(t - \tau_j)$, $\tau_1 = 32\,\delta t$, $\tau_2 = 9\,\delta t$, and $\delta t = 0.025$.

We calculated $\mathcal{C}_{uv}$ and $\mathcal{C}_{vu}$ for $u = x_1$ and $v = x_2$ in sliding windows (window duration $3000\,\delta t$ or 50 pseudoperiods, window shift $1000\,\delta t$) and show these results in Fig. 1 (middle panel).

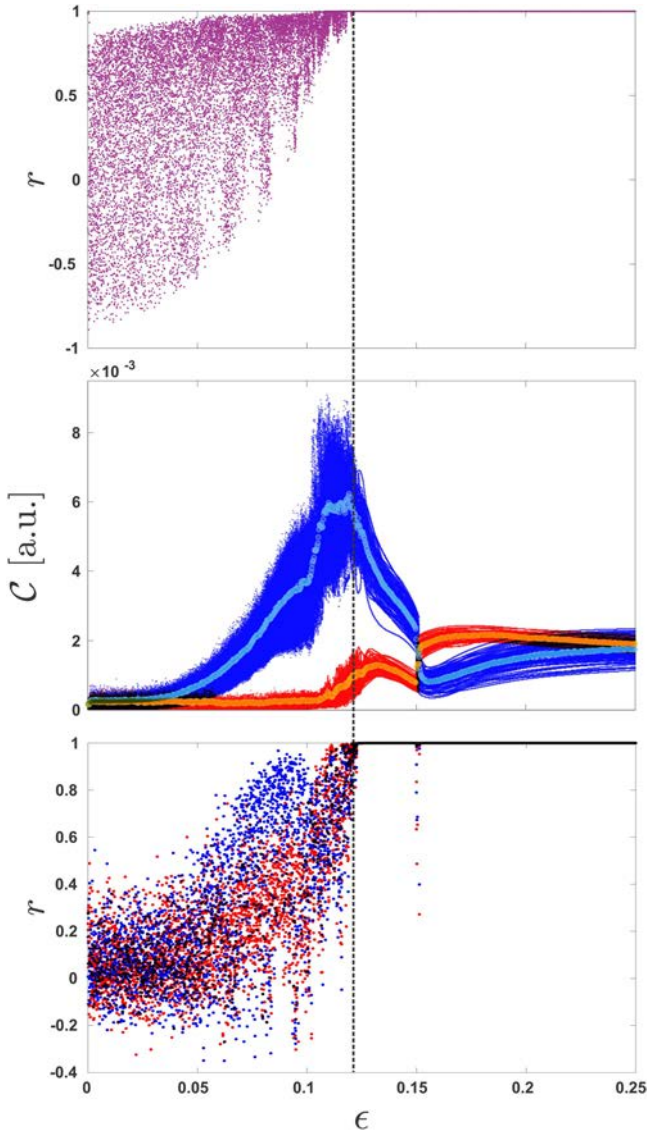

FIG. 1. Pearson correlation r between response system components x_2 (system $\boldsymbol{R_2}$) and x_3 (system $\boldsymbol{R_3}$) for determining the onset of synchronization (dashed line) between $\boldsymbol{R_1}$ and $\boldsymbol{R_2}$ (upper panel). Cross-dynamical measures for a driven periodic Rössler system by a chaotic Rössler system across coupling strength, ϵ. For each coupling strength, 97 time windows are plotted as dots. Blue dots indicate chaotic driving periodic ($\mathcal{C}_{vu}$), and red dots periodic driving chaotic ($\mathcal{C}_{uv}$) (middle panel). The average across time windows for each coupling strength is overlaid in cyan and orange. Pearson correlation between $\mathcal{C}_{uv}$ across time windows for ϵ_k and ϵ_{k+1} in red and for $\mathcal{C}_{vu}$ in blue. Both values converge to one after the onset of generalized synchronization.

Each coupling strength displays $\mathcal{C}_{vu}$ for all time windows in the direction of $u = x_1$ to $v = x_2$ (blue dots) and $\mathcal{C}_{uv}$ in the direction of v to u (red dots). $\mathcal{C}_{vu}$ increases with increasing coupling strength while $\mathcal{C}_{uv}$ remains close to zero and begins to increase around the

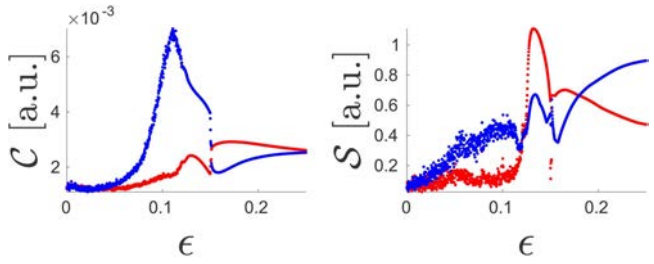

FIG. 2. Effect of short time windows: the left plot shows the CD-DDA causality measures $\mathcal{C}_{uv}$ and $\mathcal{C}_{vu}$ ($u = x_1, v = x_2$) for system (9) for a window length of 300 δt, or 5 pseudoperiods. This plot can be compared to the middle panel in Fig. 1. The right plots show our synchronization measure or significances $\mathcal{S}_{uv}$ and $\mathcal{S}_{vu}$ for the maximum of the additional three DDA parameters.

onset of generalized synchronization (GS), estimated as ϵ=0.12 in previous work based on conditional Lyapunov exponents[24] and based on the auxiliary systems approach[1] as shown in Fig. 1, upper panel. GS occurs in nonidentical, unidirectionally coupled oscillators when there is a map between trajectories on the driving attractor and trajectories on the response attractor.[29] The auxiliary systems approach requires introducing a second response system $\boldsymbol{R_3}$ [with the variables (x_3, y_3, z_3)] that is identical to $\boldsymbol{R_2}$, except for initial conditions. To determine the onset of synchronization between $\boldsymbol{R_1}$ and $\boldsymbol{R_2}$, we see when the two driven response systems undergo complete synchronization or when the Pearson correlation between x_2 and x_3 is 1 (Fig. 1, upper panel). We can also estimate the onset of generalized synchronization by correlating $\mathcal{C}_{uv}$ for ϵ_k with ϵ_{k+1} across all time windows, and doing the same for $\mathcal{C}_{vu}$ (Fig. 1, lower panel). After the onset of synchronization, neighboring ϵ values share the same synchronized manifold, whereas before, neighboring ϵ values follow distinct driven attractors.

In Fig. 2 (left panel), we investigate the effect of short time windows (see also Fig. S1 in the supplementary material). While the main effect of $\mathcal{C}_{vu}$ remains for even just five pseudoperiods, we also see $\mathcal{C}_{uv}$ unexpectedly increase before the onset of generalized synchronization.

In Fig. 2 (right panel), we show the onset of generalized synchronization in a purely data driven manner: first, we estimate the significances for the three additional, cross DDA parameters of $\mathcal{F}_v$ and $\mathcal{F}_u$ in Eqs. (6) and (7). Then, we recalculate the significance measures for two slightly different window lengths ($300 \pm 20\,\delta t$). When the two time series u and v are not synchronized, trajectories on the driving and driven attractors are unrelated, and different window lengths will yield similar significance measures. If the time series are synchronized, then there is a map between trajectories on the driving and driven attractors, and measures of significance will be sensitive to window length. To assess synchronization, we take the maximum of the three DDA parameters that shows the greatest difference across window lengths. We call this our measure of synchronization, $\mathcal{S}$.

We are able to recover the correct direction of causal inference for coupling between 0.05 and 0.15 for the longer (Fig. 1, middle panel) and shorter (Fig. 2, left panel) data windows, as well as after adding 20 dB noise (see Fig. S1 in the supplementary material).

B. Rössler system driving Lorenz system

In this example, we unidirectionally drove a Lorenz system $\boldsymbol{L}$ with a Rössler system $\boldsymbol{R}$[23]

$$\begin{aligned} \boldsymbol{R}\begin{cases} \dot{x}_1 = -\alpha(y_1 + z_1), \\ \dot{y}_1 = \alpha(x_1 + a y_1), \\ \dot{z}_1 = \alpha(b + z_1(x_1 + c)), \end{cases} \\ \boldsymbol{L}\begin{cases} \dot{x}_2 = \sigma(-x_2 + y_2), \\ \dot{y}_2 = R x_2 - y_2 - x_2 z_2 + \epsilon y_1^2, \\ \dot{z}_2 = x_2 y_2 + \beta z_2, \end{cases} \end{aligned} \tag{11}$$

where $a = b = 0.2$, $c = -5.7$, $\sigma = 10$, $R = 28$, and $\beta = -\frac{8}{3}$.

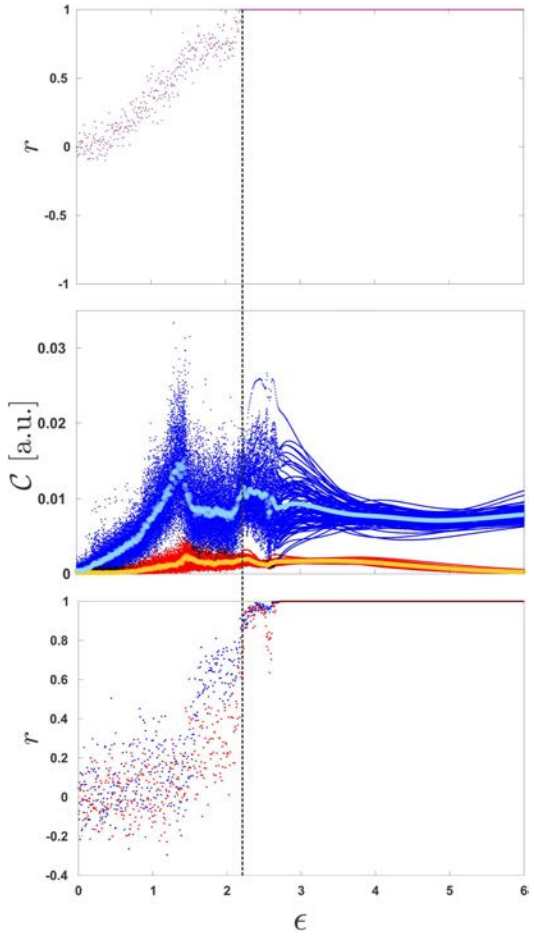

FIG. 3. Pearson correlation r between response system components y_2 (system $\boldsymbol{L}$) and y_3 (system $\boldsymbol{L_2}$) for determining onset of synchronization between $\boldsymbol{R}$ and $\boldsymbol{L}$. Cross-dynamical measures for a driven chaotic Lorenz system by a chaotic Rössler system across coupling strength, ϵ. For each coupling strength, $\mathcal{C}$ for 97 time windows are plotted as dots. Blue dots indicate $u = y_1$ driving $v = y_2$ ($\mathcal{C}_{vu}$), and red dots denote v driving u ($\mathcal{C}_{uv}$).The average across time windows for each coupling strength is overlaid in cyan and orange.

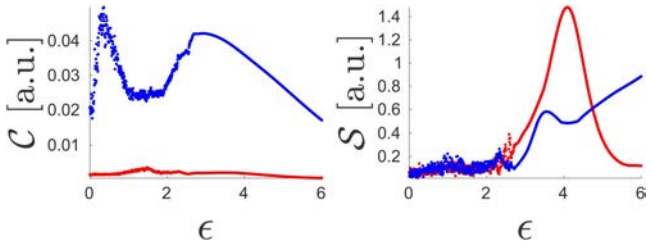

FIG. 4. Effect of short time windows: the left plot shows the CD-DDA causality measures $\mathcal{C}_{uv}$ and $\mathcal{C}_{vu}$ ($u = y_1$, $v = y_2$) for system (11). This plot can be compared to the middle panel in Fig. 3. The right plots show the significances $\mathcal{S}_{uv}$ and $\mathcal{S}_{vu}$ for the maximum of the additional three DDA parameters.

α adjusts the timescale of the Rössler system to match that of the Lorenz and is set to 6. We varied the coupling strength, ϵ, between 0 and 6 over 1000 linearly spaced values. We implemented an integration step size of 0.01, removed a transient of length 10^5, and evaluated 10^5 data points for each coupling strength. As with the coupled Rössler system, we introduce an identical copy of the response system $\boldsymbol{L}$, $\boldsymbol{L_2}$ (with components x_3,y_3, and z_3), which is also driven by $\boldsymbol{R}$ and only differs from $\boldsymbol{L}$ in initial conditions. We determined $\mathcal{F}_u$ and $\mathcal{F}_v$ for $u = y_1$ and $v = y_2$ from Eq. (12) by fitting all three-term, two-delay DDA models up to order 3 nonlinearity, scanning delays between 6 and 60 δt, and selecting the model and delays with the lowest error. This exhaustive model search was performed separately for u and v with no coupling, and is then applied to u and v for all subsequent coupling strengths

$$\begin{aligned} \mathcal{F}_u &= a_1\, u_1 + a_2\, u_2 + a_3\, u_1^2, \\ \mathcal{F}_v &= b_1\, v_1 + b_2\, v_1 v_2 + b_3\, v_1 v_2^2, \end{aligned} \tag{12}$$

where $\tau_{u,1} = 7\,\delta t$, $\tau_{u,2} = 6\,\delta t$, $\tau_{v,1} = 6\,\delta t$, and $\tau_{v,1} = 22\,\delta t$.

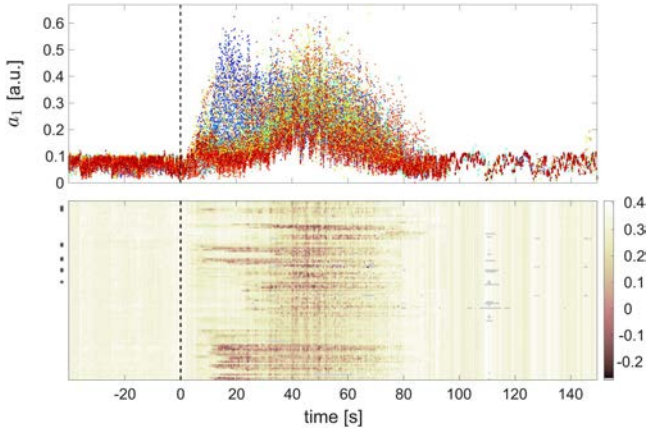

FIG. 5. Classical DDA: coefficient a_1 for 113 channels for Patient 1 in Ref. 17. In the upper panel, a_1 for each channel is shown in a different color. The lower panel shows the values of a_1 as color across all 113 channels (rows) to identify the onset channels. The onset channels marked by the neurologist are indicated by stars on the y-axis. The dotted line marks the seizure onset from the neurologist.

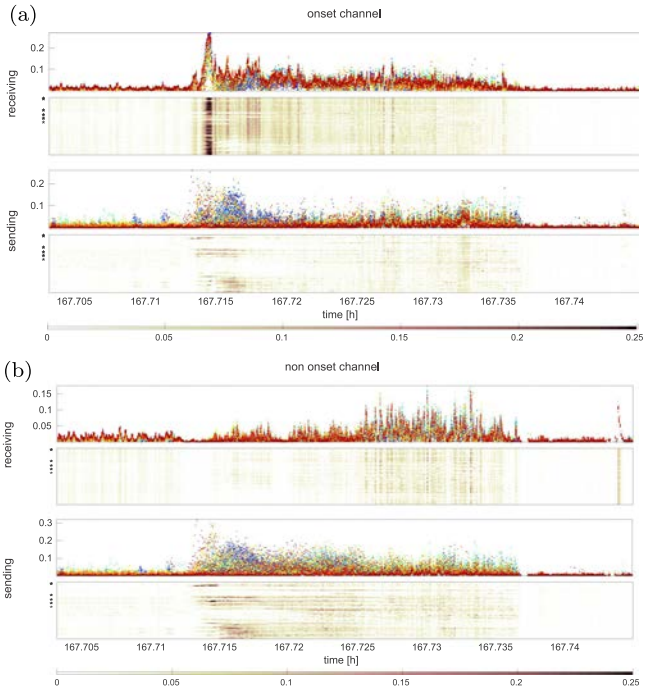

FIG. 6. CD-DDA: in the upper panels of (a) and (b), $\mathcal{C}_{vu}$ for all channels u to one channel v [onset channel in (a) and nononset channel in (b)] is shown and in the lower panels, $\mathcal{C}_{uv}$ for one channel v [onset channel in (a) and nononset channel in (b)] to all other channels u is shown. The onset channels marked by the neurologist are indicated by stars on the y-axis.

Once the models are selected, we evaluate Eq. (8) in a sliding window (window duration 3000 δt or 30 pseudoperiods, window shift 1000 δt) for each coupling strength, ϵ. In Fig. 3, each coupling strength displays $\mathcal{C}$ for all time windows in the direction of $u = y_1$ to $v = y_2$ ($\mathcal{C}_{vu}$, blue dots) and v to u ($\mathcal{C}_{uv}$, red dots). Our approach shows $\mathcal{C}_{vu}$ increases as the coupling strength increases, whereas $\mathcal{C}_{uv}$ slightly increases before the onset of GS for this system, which previous work estimates around $\epsilon = 2$,[23] and we have estimated to be $\epsilon = 2.2$ using the auxiliary systems approach. We also show in Fig. 3 lower panel the onset of synchronization by correlating $\mathcal{C}$ across time windows between ϵ_k and ϵ_{k+1}. We can also recover the correct direction of causal inference using significantly less data, that is, using 300 δt instead of 3000 δt, shown in the left panel of Fig. 4. Furthermore, we can also estimate the onset of synchronization with $\mathcal{S}_{uv}$ and $\mathcal{S}_{vu}$, as shown in the right panel of Fig. 4. Notably, $\mathcal{S}_{uv}$ in red goes up near the estimated onset of synchronization determined in Fig. 3. Overall, $\mathcal{C}$ determines the correct direction of causal inference for no noise and 20dB noise (see Fig. S3 in the supplementary material).

IV. DETECTING CAUSALITY IN EPILEPTIC SEIZURES

In Ref. 17, a genetic algorithm (GA) was used to select the model with minimum error from one second data segments for one hour periods centered on the seizure onset times. Around one million such

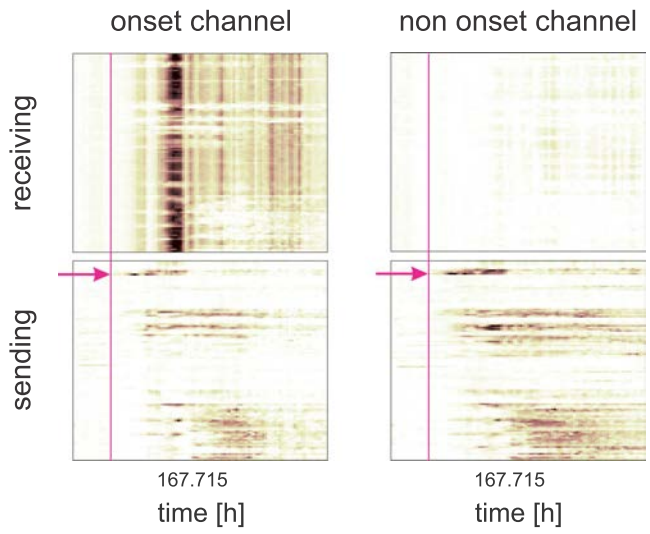

FIG. 7. CD-DDA: enlarged region around the seizure in Fig. 6.

data segments (155 seizures, 730 iEEG channels from 13 patients) were analyzed in this way. The patient demographics and characteristics are described in Ref. 17 The DDA model selected in Ref. 17 for the characterization of epileptic seizures is

$$\dot{u} = a_1 u_1 + a_2 u_2 + a_3 u_1^4 + \rho_u = \mathcal{F}_u + \rho_u, \tag{13}$$

with $u_i = u(t - \tau_i)$.

Model (13) bifurcates at the seizure onset, as shown in Ref. 17: it has a low error after seizure onset, but not before. This DDA model will be used in the remainder of this section.

In Ref. 17, eight delays were chosen to characterize and segment the data using truncated higher order SVD. In this paper, we only use the delay pair $\boldsymbol{\tau} = (7, 10)\,\delta t$, where $\delta t = \frac{1}{f_s}$ with the sampling rate $f_s = 500$ Hz since this delay pair proved to be sufficient for the characterization of epileptic seizures.

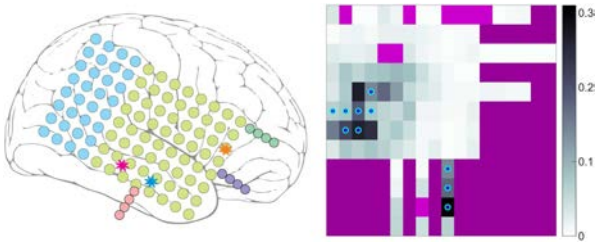

FIG. 8. The left panel shows the channel locations (for more information, see Patient 1 in Ref. 17) and the right panel shows a grid of these locations. The boxes in grayscale are the $\mathcal{C}_{uv}$ values or information sent by the onset channel to all other channels at the time of the highest peak in the upper panels in Fig. 6(a), at around 10 s after the seizure onset marked by the neurologist. The circles indicate the onset channels determined by the neurologist. The darker magenta boxes are background and the lighter magenta boxes indicate bad channels.

In Fig. 5, the coefficient a_1 from Eq. (13) is shown for 113 channels. The onset channels are marked with stars on the y-axis. As discussed in Ref. 17, these plots can be used to localize the seizure onset region in the brain.

We can extend this analysis to CD-DDA to determine the information flow patterns during seizures. $\mathcal{F}_u$ and $\mathcal{F}_v$ are the same model as Eq. (13) since all data are iEEG data. $u(t)$ and $v(t)$ are recordings from two different channels. Each channel is paired with all other channels and the information received and sent is computed for each pair.

The same seizure in Fig. 5 is shown in Fig. 6, where we show information received from all other channels (upper panels) and information sent to all other channels (lower panels) for an example onset channel (a) and for an example nononset channel (b). Figure 7 zooms into the time around seizure onset. While both channels send information to another onset channel marked with a magenta arrow just before the seizure starts, only the onset channel subsequently receives information from the majority of channels at the time of the seizure. This patient has one evoked seizure, five fully developed spontaneous seizures (first of these seizures is shown in Figs. 5–7),

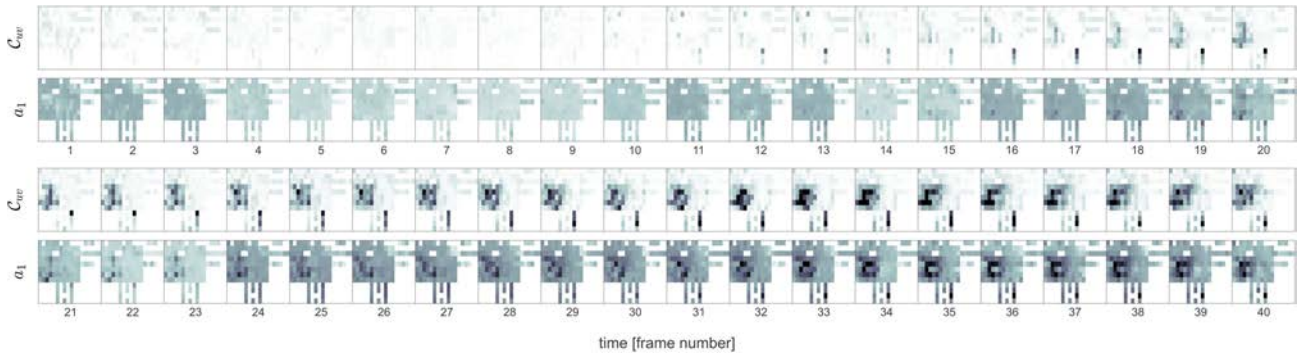

FIG. 9. Time line of the CD-DDA feature $\mathcal{C}_{uv}$ from Fig. 6(a) lower panels and the classical DDA feature a_1 from Fig. 5. The window length for each box is a quarter of a second with a window shift of half that length. The features $\mathcal{C}_{uv}$ and a_1 are mapped onto the same grid and color axis as in Fig. 8 with a white background.

and one nonfully developed seizure. In the supplementary material, we show $\mathcal{C}$ for all seizures as well as for stimulations. All spontaneous seizures except the nonfully developed one show the same signature, where the onset channel receives a large response from a majority of channels once the seizure starts. The last seizure, seizure 6, is different because the response from the nononset channels is too weak to keep the seizure developing.

In Fig. 8, the CD-DDA feature $\mathcal{C}_{uv}$ from Fig. 6 at the peak in the upper panels (around 10 s after marked onset) is mapped onto a grid (right panel) that was derived from the channel locations in the clinical report (left panel). Details and exact channel locations can be found in Ref. 17 (Patient 1). The circles denote the clinically marked onset channels. It is obvious that the region around the onset channels is sending most of the information (see also Fig. 7, magenta arrows). To investigate that further, we plotted such a grid for each sliding data window, where the window length is a quarter of a second and the window shift is half that length. Figure 9 shows such a time line for the CD-DDA feature $\mathcal{C}_{uv}$ from Fig. 6 and the classical DDA feature a_1 from Fig. 5. CD-DDA not only shows the start of the seizure earlier but also shows a constant information flow from the onset regions. Classical DDA, on the other hand, shows the generalization of the seizure and the involvement of the whole brain after seizure generalization.

V. CONCLUSION

We have developed a new tool for studying causality called CD-DDA and tested it on simulated data from dynamical systems and then further applied this technique to epileptic seizure data. Using CD-DDA, we can recover the direction of causal interaction between unidirectionally coupled systems with small parameter mismatch as well as nonequivalent systems, even with short time series and in the presence of noise (see supplementary material). Furthermore, CD-DDA can detect the onset of generalized synchronization (GS).

We have also shown that CD-DDA provides a useful measure of information flow in the brains of human patients experiencing seizures. By computing $\mathcal{C}$ for both directions for each channel, we can identify the channels that seem to be sending out information around the time of seizure onset. These channels match up well to the clinically determined onset channels. Future work will explore further applications of CD-DDA to brain data.

SUPPLEMENTARY MATERIAL

In the supplementary material, we present CD-DDA results for the simulated data from the Rössler and Lorenz systems in Sec. III for different window lengths and added white noise with a signal-to-noise ratio of SNR = 20 dB. We further show for the epilepsy patient of Sec. IV the CD-DDA outputs for 160 hours of data and plots around each of the seven seizures (from 30 s before to 2 min after seizure onset) as well as a plot for a stimulation.

ACKNOWLEDGMENTS

This work was supported by the NIH/NIBIB (Grant No. R01EB026899-01), NIH/NINDS (Grant No. R01NS104368), ONR (Grant No. N0014-15-1-2328), NIH/NINDS (Grant No. NS062092), NIH/NINDS (Grant No. NS088568), and the National Science Foundation (NSF) GRFP. The authors would like to thank Robert Kim for valuable discussions. They would also like to thank Christophe Letellier for helpful discussions and insight into working with coupled systems.

APPENDIX: EQUIVALENT RÖSSLER SYSTEMS

To remove the confusion of interpreting ω as a time scaling factor, we changed the Rössler system in Ref. 24 from

$$\begin{aligned} \dot{x} &= -\Omega y - z, \\ \dot{y} &= \Omega x + a y, \\ \dot{z} &= b + z_(x - c) \end{aligned} \tag{A1}$$

to

$$\begin{aligned} \dot{x} &= -\omega y - z, \\ \dot{y} &= x + a y, \\ \dot{z} &= b + z(x - c), \end{aligned} \tag{A2}$$

with $\omega = \Omega^2$. Both systems are exactly the same up to a scaling $y \to \Omega y$ of the y-component in the second system. As shown in Ref. 16, ω is one of the four possible bifurcation parameters of the Rössler system[27] since it can be written as[16]

$$\begin{aligned} \dot{x} &= -\frac{1}{B} y - \frac{1}{K}\frac{1}{C} z, \\ \dot{y} &= B x + a y, \\ \dot{z} &= C b - c z + K x z. \end{aligned} \tag{A3}$$

REFERENCES

[1]H. Abarbanel, N. Rulkov, and M. Sushchik, "Generalized synchronization of chaos: The auxiliary system approach," Phys. Rev. E **53**, 4528–4535 (1996).
[2]J. Arnhold, P. Grassberger, K. Lehnertz, and C. Elger, "A robust method for detecting interdependences: Application to intracranially recorded EEG," Physica D **134**(4), 419–430 (1999).
[3]E. Baek and W. Brock, "A general test for nonlinear Granger causality: Bivariate model," *Working Paper* (Korea Development Institute, University of Wisconsin-Madison, 1992), Vol. 15, pp. 197–235.
[4]Z. Bai, Y. Hui, D. Jiang, Z. Lv, W.-K. Wong, and S. Zheng, "A new test of multivariate nonlinear causality," PLoS One **13**(1), e0185155 (2018).
[5]Z. Bai, W.-K. Wong, and B. Zhang, "Multivariate linear and nonlinear causality tests," Math. Comput. Simul. **81**(1), 5–17 (2010).
[6]L. Barnett, A. B. Barrett, and A. K. Seth, "Granger causality and transfer entropy are equivalent for Gaussian variables," Phys. Rev. Lett. **103**, 238701 (2009).
[7]E. M. Bollt, J. Sun, and J. Runge, "Introduction to focus issue: Causation inference and information flow in dynamical systems: Theory and applications," Chaos **28**(7), 075201 (2018).
[8]W. Brock, W. Dechect, and J. Scheinkman, "A test for independence based on the correlation dimension," *Working Paper* (Department of Economics, 1989).
[9]W. Brock, W. Dechect, and J. Scheinkman, "A test for independence based on the correlation dimension," Econom. Rev. **15**, 197–235 (1996).
[10]C. W. Granger, "Investigating causal relations by econometric models and cross-spectral methods," Econometrica J. Econometric Soc. **37**, 424–438 (1969).
[11]P. Grassberger and I. Procaccia, "Measuring the strangeness of strange attractors," Physica D **9**, 189 (1983).
[12]C. Hiemstra and J. D. Jones, "Testing for linear and nonlinear Granger causality in the stock price-volume relation," J. Finance **49**(5), 1639–1664 (1994).
[13]Y. Hirata and K. Aihara, Identifying hidden common causes from bivariate time series: A method using recurrence plots," Phys. Rev. E **81**, 016203 (2010).
[14]Y. Hirata, J. Amigó, Y. Matsuzaka, R. Yokota, H. Mushiake, and K. Aihara, "Detecting causality by combined use of multiple methods: Climate and brain examples," PLoS One **11**, e0158572 (2016).

[15]M. Kremliovsky and J. Kadtke, "Using delay differential equations as dynamical classifiers," AIP Conf. Proc. **411**, 57 (1997).
[16]C. Lainscsek, "Nonuniqueness of global modeling and time scaling," Phys. Rev. E **84**, 046205 (2011).
[17]C. Lainscsek, J. Weyhenmeyer, S. S. Cash, and T. J. Sejnowski, "Delay differential analysis of seizures in multichannel electrocorticography data," Neural Comput. **29**(12), 3181–3218 (2017).
[18]C. Lainscsek, J. Weyhenmeyer, M. Hernandez, H. Poizner, and T. Sejnowski, "Non-linear dynamical classification of short time series of the Rössler system in high noise regimes," Front. Neurol. **4**, 182 (2013).
[19]M. Le Van Quyen, J. Martinerie, C. Adam, and F. J. Varela, "Nonlinear analyses of interictal EEG map the brain interdependences in human focal epilepsy," Physica D **127**, 250–266 (1999).
[20]E. N. Lorenz, "Deterministic nonperiodic flow," J. Atmos. Sci. **20**, 130–141 (1963).
[21]E. Miletics and G. Molnárka, "Taylor series method with numerical derivatives for initial value problems," J. Comp. Methods Sci. Eng. **4**(1–2), 105–114 (2004).
[22]N. H. Packard, J. P. Crutchfield, J. D. Farmer, and R. S. Shaw, "Geometry from a time series," Phys. Rev. Lett. **45**, 712 (1980).
[23]M. Palus, V. Komarek, Z. Hrncir, and K. Sterbova, "Synchronization as adjustment of information rates: Detection from bivariate time series," Phys. Rev. E **63**, 046211 (2001).
[24]M. Palus and M. Vejmelka, "Directionality of coupling from bivariate time series: How to avoid false causalities and missed connections," Phys. Rev. E **75**, 056211 (2007).
[25]M. Planck, "Über irreversible Strahlungsvorgänge," Ann. Phys. **306**(1), 69–122 (1900).
[26]W. Press, B. Flannery, S. Teukolsky, and W. Vetterling, *Numerical Recipes in C* (Cambridge University Press, New York, NY, 1990).
[27]O. E. Rössler, "An equation for continuous chaos," Phys. Lett. A **57**, 397 (1976).
[28]Y. Ruan, R. V. Donner, S. Guan, and Y. Zou, "Ordinal partition transition network based complexity measures for inferring coupling direction and delay from time series," Chaos **29**(4), 043111 (2019).
[29]N. Rulkov, M. Sushchik, L. Tsimring, and H. Abarbanel, "Generalized synchronization of chaos in directionally coupled chaotic systems," Phys. Rev. E **51**, 980–994 (1995).
[30]T. Sauer, J. A. Yorke, and M. Casdagli, "Embedology," J. Stat. Phys. **65**, 579 (1991).
[31]S. J. Schiff, P. So, T. Chang, R. E. Burke, and T. Sauer, "Detecting dynamical interdependence and generalized synchrony through mutual prediction in a neural ensemble," Phys. Rev. E **54**, 6708–6724 (1996).
[32]T. Schreiber, "Measuring information transfer," Phys. Rev. Lett. **85**, 461–464 (2000).
[33]G. Sugihara, R. May, H. Ye, C.-H. Hsieh, E. Deyle, M. Fogarty, and S. Munch, "Detecting causality in complex ecosystems," Science **338**(6106), 496–500 (2012).
[34]F. Takens, "Detecting strange attractors in turbulence," in *Dynamical Systems and Turbulence, Warwick 1980*, Lecture Notes in Mathematics, edited by D. A. Rand and L.-S. Young (Springer, Berlin, 1981), Vol. 898, pp. 366–381.
[35]N. Wiener, "The theory of prediction," in *Modern Mathematics for Engineers* (McGraw Hill, New York, 1956), pp. 165–190.
[36]G. U. Yule, "Why do we sometimes get nonsense-correlations between time-series? A study in sampling and the nature of time-series," J. R. Stat. Soc. **89**(1), 1–63 (1926).
[37]Y. Zou, R. V. Donner, N. Marwan, J. F. Donges, and J. Kurths, "Complex network approaches to nonlinear time series analysis," Phys. Rep. **787**, 1–97 (2019).